The 8th European Congress on Computational Methods in Applied Sciences and Engineering
ECCOMAS Congress 2022
5-9 June 2022, Oslo, Norway

AN EFFICIENT STRATEGY OF PARCEL MODELING FOR POLYDISPERSED MULTIPHASE TURBULENT FLOWS

L. BAHRAMIAN[1], J. MUELA[1,2], C. OLIET[1], C.D. PÉREZ-SEGARRA[1] AND F.X. TRIAS[1]

[1] Heat and Mass Transfer Technological Center, Technical University of Catalonia
Carrer de Colom 11, 08222 Terrassa (Barcelona), Spain; www.cttc.upc.edu

[2] Termo Fluids SL
Carrer de Magí Colet 8, 08204 Sabadell (Barcelona), Spain; www.termofluids.com

email: {linda.bahramian, jordi.muela, carles.oliet, francesc.xavier.trias, cdavid.perez.segarra}@upc.edu

Key words: Dispersed Multiphase Flows, Numerical Methods, Computational Fluid Dynamics, Lagrangian-Eulerian Method, Parcel Tracking

Abstract. A three-dimensional particle-laden two-phase turbulent flow by employing the Eulerian-Lagrangian method using multiphase Particle-In-Cell model is implemented to analyze the effects of parcel modeling. In order to achieve an optimal trade-off between accuracy and computational cost, a hybrid approach is proposed. This approach is a combination of two typical models: the volume fixed model, in which each parcel has the same volume, and the number fixed model, in which each parcel has the same number of particles. This approach is studied for the particle-laden turbulent flow benchmark case of Boreé et al. [1], with a mass loading of 22%, by using large eddy simulation through a two-way coupling between continuous and polydispersed phases.

1 INTRODUCTION

The Eulerian-Lagrangian method [2] is the best suited for dispersed multiphase flows, with a flow regime ranging from very dilute up to relatively dense with thousands or millions of particles. The Eulerian part is used for the continuous phase and the Lagrangian one for tracking the dispersed phase. This method can be applied in industrial applications, like the fuel injection of combustion chambers, cyclone separators, evaporative cooling, and dispersion of pollutants.

In order to simulate dispersed multiphase flows, the coupling level must be determined based on the total volume fraction in the system. The volume fraction is the ratio of the volume of the dispersed phases over the volume of the flow. In dilute flows, with volume fractions smaller than 10^{-6}, only the influence of the carrier phase over the dispersed phase is considered, known as one-way coupling. However, in dispersed flows with higher volume fractions, the effect of the dispersed phase over the continuous one should be considered, known as two-way coupling. This effect is commonly applied as a source term in the conservation equations of the carrier phase.

Barve et al. [3] studied the effect of co-flow velocity ratio on evolution of polydisperse particles in coaxial turbulent jets. Salehi et al. [4] presented LES of polydispersed turbulent recirculating flows using a two-way coupled probability density function of the population balance equation (PDF-PBE) for the benchmark case of Boreé et al. [1] with a mass loading of 22%.

In order to reduce the computational costs due to tracking all the individual particles, one approach consists of tracking parcels instead of particles, where each parcel represents the specified number of particles with the same properties.

Watanabe et al. [5] studied polydisperse systems with a specified particle-size distribution where two methods for arranging the particles in parcels were examined: the NFM, in which each parcel has the same number of particles, and the VFM, in which each parcel has the same volume (see Fig. 1). Employing the parcel model coupled with the Particle-In-Cell method [6] generates some discrepancies in the interaction between phases, affecting particle dispersion and interphase momentum transfer. These discrepancies grow with increasing the number of particles per parcel. Yang et al. [7] employed a three-dimensional reactive multiphase Particle-In-Cell (MP-PIC) model to investigate biomass combustion and gasification in fluidized bed furnaces based on a parcel method. They implemented a distribution kernel method (DKM) to handle the over-loading problem of MP-PIC model. They found that, for low carrier load condition, the DKM and MP-PIC model results agree with each other very well.

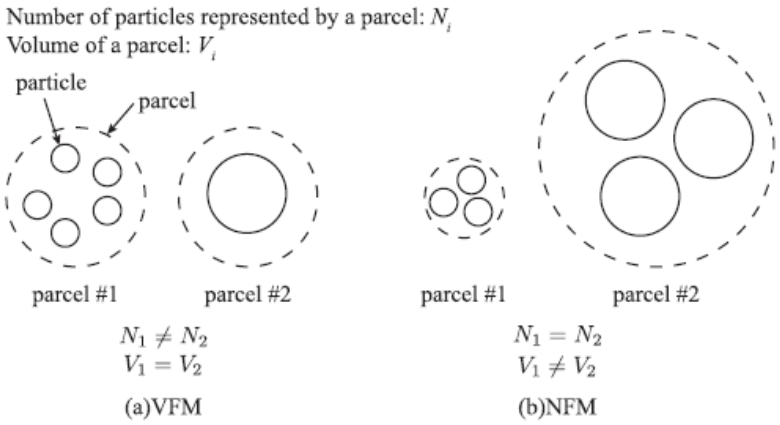

Figure 1: Schematics of parcel models. (a) VFM and (b) NFM (Figure from [5])

In the present work, a hybrid approach for parcel modeling using MP-PIC model is proposed. The objective is in addition to decrease the computational costs, the accuracy remains appropriate. The paper is organized as follows: this first section is a brief introduction. The second section gives an overview of the background necessary for understanding the numerical methods and presents the main equations besides describing the new parcel method. In the third section, the validation of numerical simulation based of the presented benchmark case is first studied. Then, the new approach is designed and after that, the results are compared with two previous parcel models, the NFM and VFM. In the last section, some conclusions are drawn.

2 NUMERICAL SIMULATION

2.1 Governing equations

The goal of this section is to summarize the essential equations and numerical methods that have been applied. The dispersed phase motion in a continuous phase using a Lagrangian method can be defined by classical equations of motion, i.e., Newton's law. The primary work in this field was employed by Basset [8], Boussinesq [9] and Oseen [10] called BBO-equation. The BBO-equation in non-uniform flow for small rigid particles was analysed with details in the work of Maxey and Riley [11]. Therefore the governing equations for determining the nth particle position and momentum are:

$$\frac{\mathrm{d}\mathbf{x_p^n}}{\mathrm{d}t} = \mathbf{v_p^n} \tag{1}$$

$$m_\mathrm{p}^n \frac{\mathrm{d}\mathbf{v_p^n}}{\mathrm{d}t} = \sum_i \mathbf{F_i} \tag{2}$$

where $\mathbf{x_p^n}$, $\mathbf{v_p^n}$, and m_p^n are the nth particle's center location, velocity, and mass. The sum of forces appearing on the right-hand side of Eq. (2) accounts for all the relevant forces acting over the particles, e.g., drag, gravity, added mass, pressure gradient force, etc.

It is assuming that particles are large enough that any Brownian or non-continuum motion of the particles may be neglected. Thus, Eq. (2) under influence of drag and gravity and buoyancy forces can be expressed as:

$$m_\mathrm{p}^n \frac{\mathrm{d}\mathbf{v_p^n}}{\mathrm{d}t} = \frac{1}{2}\rho_\mathrm{c} C_D A_\mathrm{p}^n \left|\mathbf{u}(\mathbf{x_p^n}) - \mathbf{v_p^n}(\mathbf{x_p^n})\right| \left(\mathbf{u}(\mathbf{x_p^n}) - \mathbf{v_p^n}(\mathbf{x_p^n})\right) + \left(1 - \frac{\rho_\mathrm{c}}{\rho_\mathrm{p}}\right) m_\mathrm{p}^n \mathbf{g} \tag{3}$$

where ρ_c and ρ_p are the density of the fluid (assumed constant) and the density of the particle. C_D is the drag coefficient, A_p^n, the particle cross-section area, $\mathbf{g}$, gravitational acceleration vector and $\mathbf{u}(\mathbf{x_p^n})$ is the fluid's velocity in the nth particle's position.

Numerical approximation of the fluid velocity at the particle position $\mathbf{u}(\mathbf{x_p^n})$ is determined by interpolating the fluid velocity from a stencil of surrounding nodes. Hence, these interpolations can be seen as a weighted sum of the velocities in the computational nodes surrounding particle position.

According to the fact that the volume fraction of particles is relatively small (i.e., less than 0.1%), the volume that the particle phase occupies can be neglected (i.e., dilute approximation). For dense dispersed two-phase flow, Elghannay et al. [12] implemented a partial coupling techniques by neglecting the explicit effect of void fraction in the fluid momentum equations while retaining its effect on force models. For simplicity, it is assumed that the drag force is the only significant fluid-particle interaction force in the two-way coupling between particles and fluid. The equations of a viscous incompressible continuous fluid are governed by the Navier-Stokes (NS) equations and detailed by Sagaut [13]. It can be approximated by:

$$\nabla \cdot \mathbf{u} = 0 \tag{4}$$

$$\rho_\mathrm{c}\left[\frac{\partial \mathbf{u}}{\partial t} + \nabla \cdot (\mathbf{u}\mathbf{u})\right] = -\nabla p + \mu \nabla^2 \mathbf{u} + \mathbf{S_u} \quad , \quad \mathbf{S_u} = -\sum_{n=1}^{N_\mathrm{p}} \frac{m_\mathrm{p}^n \mathbf{f_{cp}^n}}{V_\mathrm{cell}} \tag{5}$$

where p, μ, and $\mathbf{S_u}$ are the pressure, the dynamic viscosity, and the momentum source term. $\mathbf{f}_{\mathrm{cp}}^{\mathbf{n}}$, V_{cell}, and N_p are the fluid-particle interaction force per unit mass of the particle, the volume of the computational cell, and the number of particles occupying in a computational cell.

2.2 Parcel modeling

As mentioned earlier, the typical two types of parcel models are the NFM and the VFM (see Fig. 1). According to the results presented by Watanabe et al. [5], the discrepancies in the utilization of the parcel model with the number of particles per parcel, N_p, in $\mathcal{O}(10^0)$ would be acceptable, whereas those with N_p in $\mathcal{O}(10^1)$ significantly affect the results and the parcel model should be carefully treated with confirming N_p in the entire range of the particle size distribution. It is found that the VFM cannot predict accurately the particle dispersion characteristics for the particles with diameters smaller than the Sauter mean diameter, SMD. This is happening because the number of particles is represented by one parcel are much higher than the NFM. Also, with increasing the number of particles per parcel, the NFM cannot present good results for the particles with diameters bigger than the SMD. This is because the parcels have much bigger volume than the VFM.

Therefore, a new approach is proposed to achieve good results with the possibility of increasing N_p in the $\mathcal{O}(10^1)$ for some range of particles. This approach is a combination of the previous two methods, in which the particles with diameters below the SMD are arranged with the NFM, and the particles with diameters above the SMD are arranged with the VFM. A schematic of this proposal is shown in Fig. 2. As is shown in Fig. 2, the parcels on the right-hand side of the SMD, which include particle diameters above the SMD, are arranged by the VFM. In addition, the parcels on the left-hand side of the SMD, which consist of particle diameters below the SMD, are arranged with the NFM.

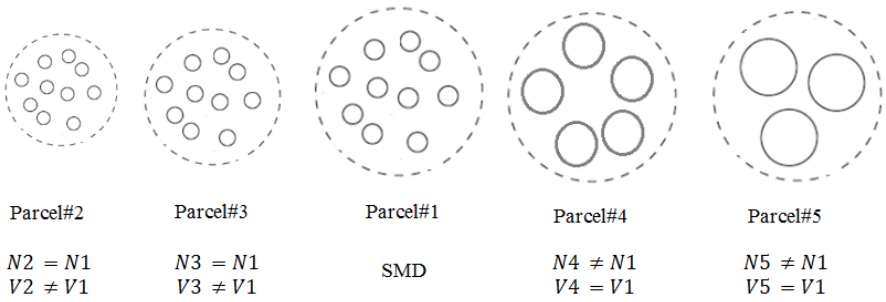

Figure 2: Schematic of the new parcel model

The SMD, in terms of a finite number of discrete size classes is defined as [14]:

$$D_{pq} = \left[\frac{\sum_{i=1}^{\infty} n_i D_i^p}{\sum_{i=1}^{\infty} n_i D_i^q} \right]^{1/(p-q)} \tag{6}$$

where $p = 3$ and $q = 2$. n and D are the number distribution and the diameter of the particle sizes, respectively.

3 RESULTS AND DISCUSSION

A real test case of a particle-laden turbulent flow in the framework of LES and through the Wall-adapting eddy viscosity (WALE) turbulent model is carried out. The dispersed multiphase flow is modeled using the Eulerian-Lagrangian method assuming two-way coupling between the continuous and the dispersed phase. The selected benchmark case, shown in Fig. 3, is the flow loop Hercule of Borée et al. [1] with a mass loading ratio in the inner jet of 22% (M=22%), which generates an axisymmetric confined bluff body flow. Particles are ordered with the mean diameter class of 20, 30, 40, 50, 60, 70, 80, 90, 100μm. All the numerical simulations performed in this work have been carried out using an in-house parallel c++/MPI CFD code called TermoFluids [16] based on the finite volume method (FVM) and symmetry-preserving discretization of the momentum equation. Berrouk [17] presented a detailed stochastic LES of this benchmark case through the Eulerian-Lagrangian method for two mass loading ratio in the inner jet of 22% and 110% (M=22%, M=110%) using the open-source code Code_Saturne. Greifzu et al. [18] used this benchmark case (M=22%) for Comparing open-source code OpenFOAM and ANSYS FLUENT using the Eulerian-Lagrangian method in the framework of RANS turbulent model.

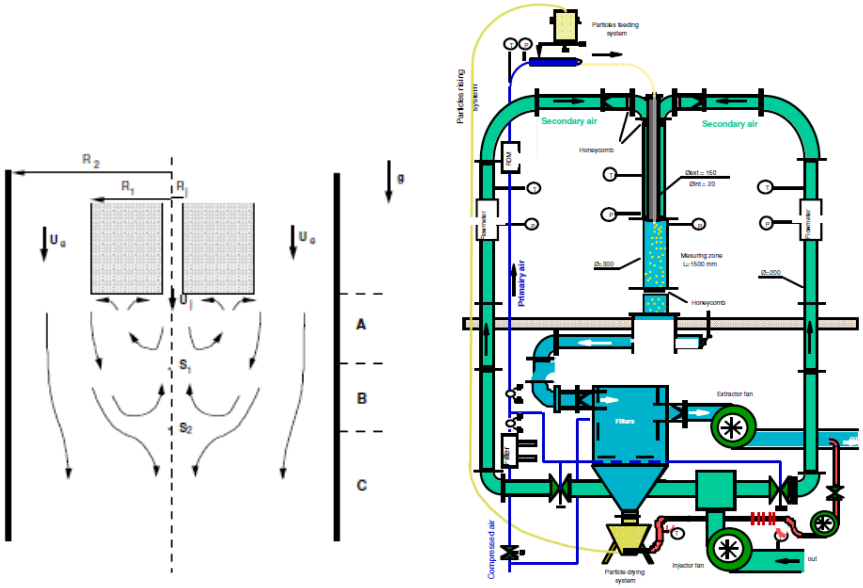

(a) (b)

Figure 3: (a) Sketch of the confined bluff body flow and (b) Schematic drawing of the Hercule flow loop (Figures from [15])

3.1 Validation

First of all, a validation of the numerical simulation according to the experimental data by Borée et al. [1] is carried out by tracking all the individual particles (no-parcel).

Fig. 4 and Fig. 5 show the radial mean streamwise velocity profiles of carrier and dispersed phase ($d_p = 20\mu m$) at the different sections of the domain perpendicular to the direction of the

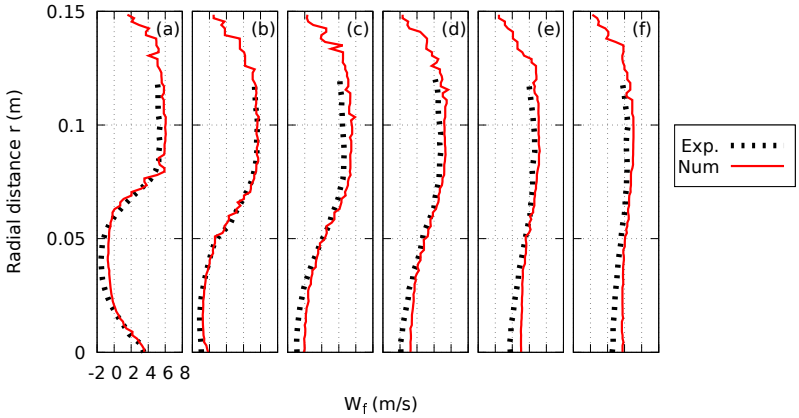

Figure 4: Radial profiles of fluid mean streamwise velocity for particle-laden configuration (M=22%). Circle: Experiment [1]; solid line: Numerical simulation. (a) z=0.08m; (b) z=0.16m; (c) z=0.20m; (d) z=0.24m; (e) z=0.32m; (f) z=0.40m

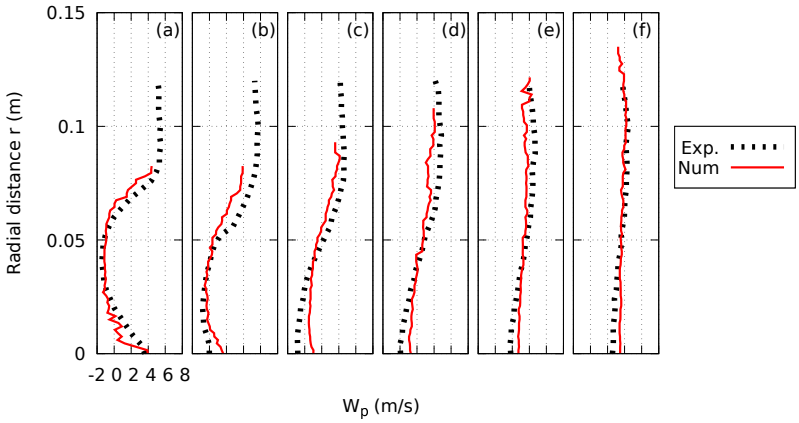

Figure 5: Radial profiles of particle ($dp = 20\mu m$) mean streamwise velocity for particle-laden configuration (M=22%). Circle: Experiment [1]; solid line: Numerical simulation. (a) z=0.08m; (b) z=0.16m; (c) z=0.20m; (d) z=0.24m; (e) z=0.32m; (f) z=0.40m

flow. As can be observed, the numerical simulation is in good agreement with the experimental data, both for the fluid and for the particles.

3.2 Designing new approach

The first step for designing the new approach is defining the number of particles per parcel considering the SMD. Then, for the particles with a diameter above the SMD, arrange the number of particles per parcel by fixing the parcel volume equal to the one corresponding to the SMD's (using the VFM), and for the particles with a diameter below the SMD, fixing the

number of particles per parcel equal to the one correspondig to the SMD's (using the NFM).

As mentioned before, by increasing the number of particles per parcel, the NFM, cannot present good results for the bigger particles than the SMD. Thus, one approach will be increasing the number of particles per parcel using NFM and comparing the results, especially for the particles with diameters above the SMD. The SMD calculated for this test case is 60 μm.

The results for the particles equal and above the SMD with setting the number of particles per parcel to 5, 10, and 20 are shown in Figs. 6, 7 and 8. As can be seen, the parcels with particles of 100μm diameter start to show some disagreements from NFM_{10} (the subindex indicates the number of particles per parcel), the parcels with particles of 80μm and 90μm diameters are showing some discrepancies from NFM_{20}.

According to these results, for $dp = 80\mu m$ the appropriate number of particles per parcel is between 10 and 20. Thus, by using VFM between $dp = 80\mu m$ and the SMD ($dp = 60\mu m$), the number of particles per parcel for SMD for designing the new models is set to 40. Table 1 presents the parcel types selected for the particle size distribution in this model. The number and volume of parcels allocated to each particle size are shown in Fig. 9 and Fig. 10.

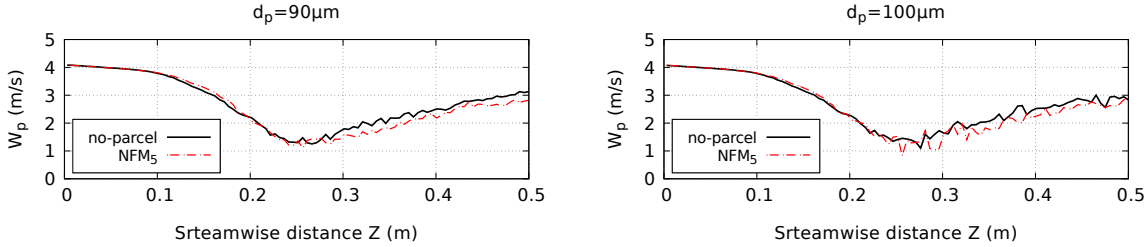

Figure 6: Streamwise profiles of particle ($dp = 90\mu m$ and $dp = 100\mu m$) for the particle-laden configuration (M=22%) comparing no-parcel and NFM_5.

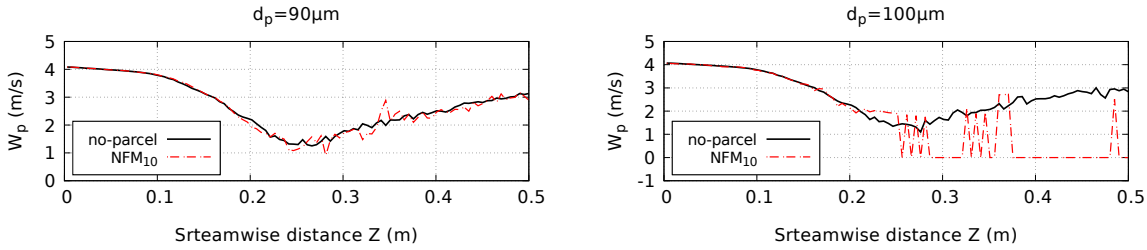

Figure 7: Streamwise profiles of particle ($dp = 90\mu m$ and $dp = 100\mu m$) for the particle-laden configuration (M=22%) comparing no-parcel and NFM_{10}.

3.3 Comparing the parcel models

This section presents the results obtained for the new proposed hybrid model compared with the NFM and the VFM. The objective here is to see if the hybrid model can present better

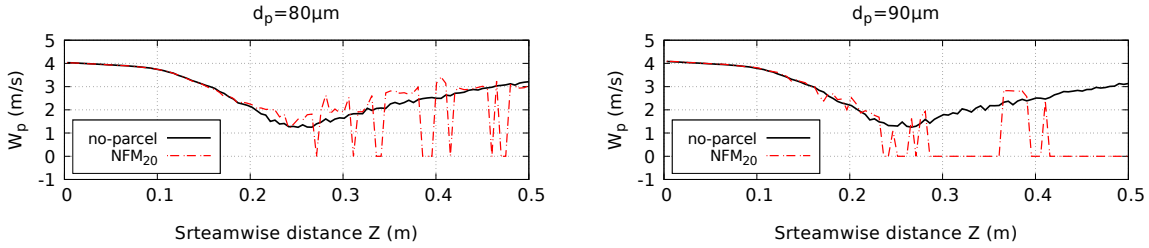

Figure 8: Streamwise profiles of particle ($dp = 80\mu m$ and $dp = 90\mu m$) for the particle-laden configuration (M=22%) comparing no-parcel and NFM_{20}.

Table 1: Defining parcel type model according to particle diameter distribution

***dp*(μm)**	20	30	40	50	60	70	80	90	100
Parcel Type	NFM	NFM	NFM	NFM	NFM/VFM	VFM	VFM	VFM	VFM

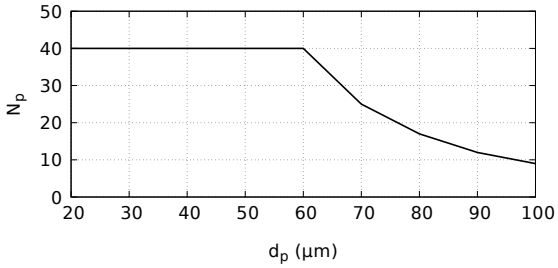

Figure 9: Number distribution of particles per parcel regarding to the particle size

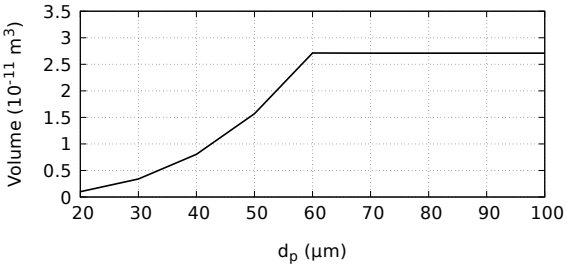

Figure 10: Volume distribution of parcels allocated to the particle size

behavior than the VFM for the particles with diameters smaller than the SMD, along with showing fewer discrepancies than the NFM for the particles with diameters above the SMD. Therefore, for some selected particles with diameters below and above the SMD, the mean velocity profiles of the dispersed phase are presented.

In order to compare the hybrid model with the VFM, the particles with diameters $dp = 20\mu m$ and $dp = 30\mu m$ have been selected. Fig. 11 shows the streamwise mean velocity profiles of the parcels with particle diameter of $dp = 30\mu m$. As can be seen, the hybrid model is showing less discrepancies than the VFM regarding to the no-parcel model. Also in Fig. 12 which shows the radial profile of particle mean velocity ($dp = 20\mu m$), the hybrid model follows better the no-parcel model than the VFM. In this figure, the zero velocities show that no parcel is allocated to that specific control volume. Therefore, for parcels with particle diameters of $dp = 20\mu m$,

the hybrid model shows better parcel dispersion than the VFM in the MP-PIC model.

For comparing the hybrid model with the NFM, the particles with diameters $dp = 80\mu m$ and $dp = 90\mu m$ were selected. In Fig. 13 the streamwise mean velocity profiles of the dispersed phase are presented. As can be observed, for the particle diameters above the SMD ($dp = 80\mu m$ and $dp = 90\mu m$), the hybrid model is showing much less discrepancies than the NFM compared with the no-parcel model. It can be seen that the NFM is showing lots of zero velocities meaning that there is no parcel allocated in those specific cells. Fig. 14 presents the radial mean velocity profiles in different cross-section of the domain. It can be observed that for these particle diameters, the hybrid model can obtain better particle dispersion than the NFM according to the no-parcel model.

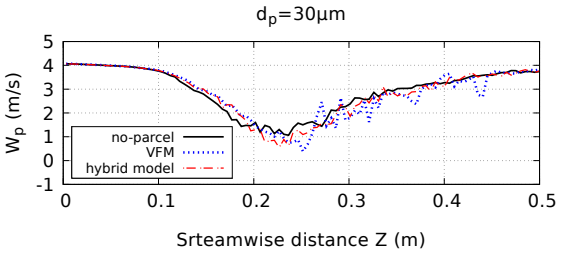

Figure 11: Streamwise profiles of particle ($dp = 30\mu m$) for the particle-laden configuration (M=22%) comparing no-parcel, VFM and hybrid model.

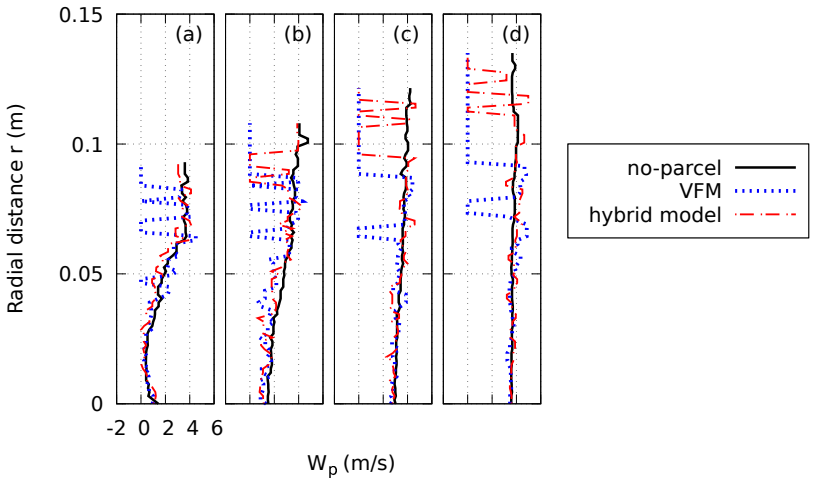

Figure 12: Radial profiles of particle ($dp = 20\mu m$) mean streamwise velocity for particle-laden configuration (M=22%). (a) z=0.20m; (b) z=0.24m; (c) z=0.32m; (d) z=0.40m

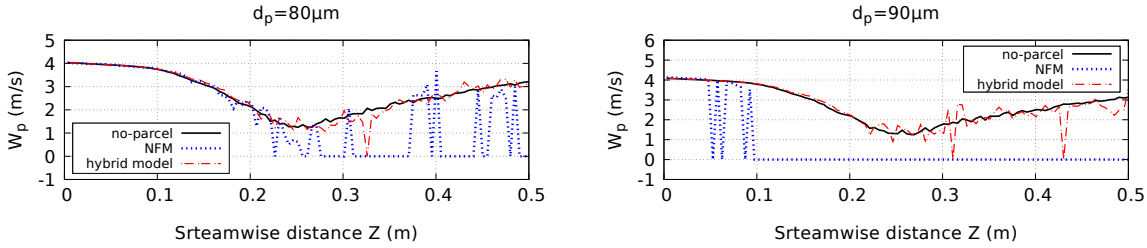

Figure 13: Streamwise profiles of particle ($dp = 80\mu m$, $dp = 90\mu m$) for the particle-laden configuration (M=22%) comparing no-parcel, NFM and hybrid model.

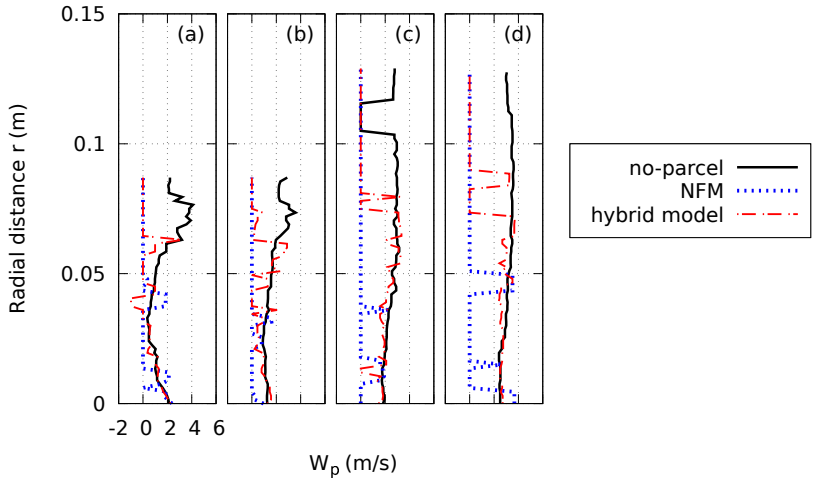

Figure 14: Radial profiles of particle ($dp = 80\mu m$) mean streamwise velocity for particle-laden configuration (M=22%). (a) z=0.20m; (b) z=0.24m; (c) z=0.32m; (d) z=0.40m

4 CONCLUSIONS

- The present work is focused on the study and development of a new approach for parcel modeling based on a combination of the NFM and VFM according to the SMD.
- The benchmark case of Borée et al. [1] was chosen as a validation test case of the no-parcel model because it contains multiple complex flow characteristics which are typical of combustion chambers.
- The MP-PIC scheme was used to model the two-way coupling between the continous and despersed phase in the framework of LES through the WALE model.
- This test case was an opportunity to evaluate the handling of two-way coupling in the in-house CFD code TermoFluids [16].

- Numerical results on mean radial velocities for both continuous and dispersed phase show very good agreement with the experimental findings.
- The hybrid parcel model is designed based on the analysis of the NFM for the particle diameters above the SMD.
- This hybrid model uses the NFM for the particle diameters below the SMD, and the VFM for the particle diameters above the SMD.
- For the particle diameters below and equal to the SMD, N_p has been increased in the $\mathcal{O}(10^1)$.
- In comparison with the no-parcel model, for the particle diameters below the SMD, the hybrid model shows better parcel dispersion and fewer discrepancies in the mean velocity profile of the dispersed phase (both in streamwise and radial profiles) than the VFM.
- Observing the results of the no-parcel model, for the particle diameters above the SMD, this hybrid model presents better agreement and fewer discrepancies in the mean velocity profile of the dispersed phase (both in streamwise and radial profiles) than the NFM.
- In conclusion, according to the presented preliminary results of the hybrid parcel model compared with the previous models: the NFM and the VFM, in addition to decreasing the computational cost, the accuracy remains appropriate.
- Further analyses of particle dispersion and particle volume fraction can be implemented for the hybrid model.

ACKNOWLEDGEMENTS

Linda Bahramian acknowledges the financial support from the Secretariat of Universities and Research of the Generalitat de Catalunya and the European Social Fund, FI AGAUR Grant (2019 FI_B 01205). Carles Oliet, as a Serra Húnter lecturer, acknowledges the Catalan Government for the support through this Programme.

REFERENCES

[1] Borée, J., Ishima, T. and Flour, I. The effect of mass loading and inter-particle collisions on the development of the polydispersed two-phase flow downstream of a confined bluff body *Journal of Fluid Mechanics*. (2001) **443**:129-165.

[2] Subramaniam, S. Lagrangian–Eulerian methods for multiphase flows. *Progress in Energy and Combustion Science*. (2013) **39(2-3)**:215-245.

[3] Barve, A.V., Sahu, S. and Anupindi, K. Effect of co-flow velocity ratio on evolution of poly-disperse particles in coaxial turbulent jets: A large-eddy simulation study. *Physics of Fluids*. (2020) **32(9)**:093303.

[4] Salehi, F., Cleary, M.J., Masri, A.R. and Kronenburg, A. Large eddy simulation of polydispersed inertial particles using two-way coupled PDF-PBE. *International Journal of Heat and Fluid Flow*. (2020) **83**:108585.

[5] Watanabe, H., Uesugi, D. and Muto, M. Effects of parcel modeling on particle dispersion and interphase transfers in a turbulent mixing layer. *Advanced Powder Technology*. (2015) **26(6)**:1719-1728.

[6] Crowe, C.T., Sharma, M.P., Stock, D.E. The Particle-Source-in-Cell (PSI-CELL)model for gas-droplet flows. (1977) 325–332.

[7] Yang, M., Zhang, J., Zhong, S., Li, T., Løvås, T., Fatehi, H. and Bai, X.S. CFD modeling of biomass combustion and gasification in fluidized bed reactors using a distribution kernel method. *Combustion and Flame*. (2022) **236**:111744.

[8] Basset, A.B. On the motion of a sphere in a viscous liquid. *Philosophical Transactions of the Royal Society of London A: Mathematical, Physical and Engineering Sciences*. (1888) **179**:43-63.

[9] Boussinesq, J. Sur la resistance qu'oppose un fluide indefini en repos, sans pesanteur, au mouvement varie d'une sphere solide qu'il mouille sur toute sa surface, quand les vitesses restent bien continues et assez faibles pour que leurs carres et produits soient negligiables. *CR Acad. Sc. Paris*. (1885) **100**:935-937.

[10] Oseen, C.W. Hydrodynamik. *Akademische Verlagsgesellschaft*. (1927).

[11] Maxey, M.R. and Riley, J.J. Equation of motion for a small rigid sphere in a nonuniform flow. *The Physics of Fluids*. (1983) **26(4)**:883-889.

[12] Elghannay, H.A. and Tafti, D.K., 2018. Revised partial coupling in fluid–particulate systems. *The Journal of Computational Multiphase Flows*. (2018) **10(4)**:215-227.

[13] Sagaut, P. Large eddy simulation for incompressible flows: an introduction. *Springer Science Business Media*. (2006).

[14] Azzopardi, B.J. Sauter mean diameter. *Thermopedia, [Online]. Available: http://www.thermopedia.com/content/1108/. [Accessed 01 03 2013]*. (2011).

[15] Ishima, T., Borée, J., Fanouillère, P. and Flour, I. Presentation of a two phase flow data base obtained on the flow loop Hercule. *In 9th Workshop on Two-phase Flow Predictions*. (1998).

[16] Termo Fluids S.L., Termofluids. *http://www.termofluids.com/*. (2020).

[17] Berrouk, A.S. Stochastic Large Eddy Simulation of an Axisymmetrical Confined-Bluff-Body Particle-Laden Turbulent Flow. *American Journal of Fluid Dynamics*. (2012) **2(6)**:101-116.

[18] Greifzu, F., Kratzsch, C., Forgber, T., Lindner, F. and Schwarze, R. Assessment of particle-tracking models for dispersed particle-laden flows implemented in OpenFOAM and ANSYS FLUENT. *Engineering Applications of Computational Fluid Mechanics*. (2016) **10(1)**:30-43.